FEBS Letters

FEBS PRESS science publishing by scientists

Metabolite systems profiling identifies exploitable weaknesses in retinoblastoma

Swagatika Sahoo[1,2], Ranjith Kumar Ravi Kumar[3], Brandon Nicolay[4,†], Omkar Mohite[2,5,‡], Karthikeyan Sivaraman[6], Vikas Khetan[7], Pukhraj Rishi[7], Suganeswari Ganesan[8], Krishnakumar Subramanyan[8], Karthik Raman[2,5,9], Wayne Miles[4,10] and Sailaja V. Elchuri[3]

1 Department of Chemical Engineering, Indian Institute of Technology Madras, Chennai, India
2 Initiative for Biological Systems Engineering, Indian Institute of Technology Madras, Chennai, India
3 Department of Nanotechnology, Vision Research Foundation, Sankara Nethralaya, Chennai, India
4 Department of Molecular Oncology, Massachusetts General Hospital Cancer Center and Harvard Medical School, Charlestown, MA, USA
5 Department of Biotechnology, Bhupat and Jyoti Mehta School of Biosciences, Indian Institute of Technology Madras, Chennai, India
6 Medgenome Labs, Bangalore, India
7 Shri Bhagwan Mahavir Vitreoretinal Services and Ocular Oncology Services, Sankara Nethralaya, Chennai, India
8 Department of Histopathology, Vision Research Foundation, Sankara Nethralaya, Chennai, India
9 Robert Bosch Centre for Data Science and Artificial Intelligence (RBC-DSAI), Indian Institute of Technology Madras, Chennai, India
10 Department of Molecular Genetics, The Ohio State University Comprehensive Cancer Center, The Ohio State University, Columbus, OH, USA

Correspondence
S. Sahoo, Department of Chemical Engineering, Indian Institute of Technology Madras, Chennai 600036, India
Fax: +91 4422574150
Tel: +91 4422574189
E-mail: swagatika05@gmail.com
and
S. V. Elchuri, Department of Nanotechnology, Vision Research Foundation, Sankara Nethralaya, Chennai 600006, India
Fax: +91 4428254180
Tel: +91 4428271616
E-mail: sailaja.elchuri@gmail.com

Present addresses
†Agios Pharmaceutical, 88 Sidney Street, Cambridge, MA, USA

‡The Novo Nordisk Foundation Center for Biosustainability, Technical University of Denmark, Kongens Lyngby, Denmark

(Received 1 June 2018, revised 25 September 2018, accepted 6 November 2018, available online 27 November 2018)

doi:10.1002/1873-3468.13294

Edited by Alfonso Valencia

Retinoblastoma (RB) is a childhood eye cancer. Currently, chemotherapy, local therapy, and enucleation are the main ways in which these tumors are managed. The present work is the first study that uses constraint-based reconstruction and analysis approaches to identify and explain RB-specific survival strategies, which are RB tumor specific. Importantly, our model-specific secretion profile is also found in RB1-depleted human retinal cells *in vitro* and suggests that novel biomarkers involved in lipid metabolism may be important. Finally, RB-specific synthetic lethals have been predicted as lipid and nucleoside transport proteins that can aid in novel drug target development.

Keywords: cancer metabolism; constraint-based reconstruction and modeling; retinoblastoma; synthetic lethal; systems biology

Abbreviations
COBRA, constraint-based reconstruction and analysis; FBA, flux balance analysis; GABA, gamma-aminobutyric acid; RB, retinoblastoma; SRM, selected reaction monitoring.

The retina is a metabolically active tissue that preferentially uses carbohydrates (i.e., glucose and mannose) for energy [1]. In addition, extensive lipid metabolism (e.g., fatty acid metabolism) and vitamin metabolism (e.g., vitamin A and pteridine metabolism), along with specialized amino acid metabolism (e.g., glutamate metabolism and urea cycle), make retinal tissue unique from the rest of the central nervous system. Retinoblastoma (RB) is caused by the loss of RB1 (GeneID: 5925, *RB1*) function [2]. It is a childhood tumor affecting one or both eyes with an incidence of 1 in 15 000 to 20 000 births [3–5]. Due to late-stage presentation, mortality is higher in Asia and Africa (35–73%), when compared to United States (5–13%) [5–7]. Additionally, patients with germ line mutation are prone to secondary cancers compared to the general population [8]. The medical management for RB involves predominantly chemotherapy, that is, systemic chemotherapy with triple chemotherapy drugs like carboplatin, etoposide, and vincristine. Currently, intravitreal chemotherapy with melphalan and intra-arterial chemotherapy with carboplatin are commonly practiced to save the vision of these children. If these measures fail, enucleation is done [9,10]. However, both enucleation and chemotherapy have severe side effects, including intellectual and developmental disabilities [11–13]. Recently, metabolomics on RB samples identified a number of metabolites (majorly from amino acid and lipid metabolism), concentrations of which significantly differed from healthy tissue [14]. This highlights the role of retinoblastoma-specific metabotype and its potential for explaining the underlying pathology.

Constraint-based reconstruction and analysis (COBRA) remains the preferred systems biology tool to gain fundamental knowledge on the genomics and biochemistry of the target organism [15]. In line with this, the human metabolic reconstruction, that is, Recon [16–18], has been published accounting for metabolic reactions and their associated enzymes/genes operating in any given human cell. Recon serves as a knowledge base for interrogating human metabolism within any given disease context [19,20]. Consequently, integration of 'omics' data onto the core metabolic model helps a clearer understanding of the molecular events, (i.e., the genomic, transcriptomic, proteomic, or metabolomic factors) that drive the cancer phenotype [21]. Subsequently, algorithms exist (e.g., GIMME, iMAT, MBA, FastCore, etc.) that can integrate the 'omics' data to generate condition-specific models [22]. A number of studies have employed COBRA modeling strategy, in order to explain the cancer-specific phenotype and its underlying metabolic factors [21,23–25].

Synthetic lethality is a novel concept in cancer research, wherein, genes/reaction pairs when targeted together hinder cell viability [26]. This has been widely explored to develop treatment options with respect to cancer-specific drug targets [26–28]. Additionally, COBRA modeling approaches have enabled in identification of robust cancer-specific synthetic lethal interactions [29,30].

To date, no study exists that uses mathematical modeling to analyze the major functions of retina and their derangement in RB, from the biochemical pathways/metabolism standpoint. Here, we present a constraint-based metabolic model of RB, which uses RNAseq data of healthy as well as patient groups as constraints for generating patient-specific models from the human metabolic network, Recon 2 [17]. The generated models were used to identify the precise metabolic differences between healthy versus RB as well as between the cancer types. The RB-specific secretion profiles as predicted by the models were validated using MS/MS. Furthermore, synthetic lethals associated with RB progression were identified and novel drug targets were suggested.

Materials and methods

Obtaining gene expression data

Normal retina ($N = 3$, aged 5, 12 and 22 years) samples for RNA sequencing were obtained from PU Shah eye bank at Medical Research Foundation, Sankara Nethralaya. The RB tumors ($N = 7$) were obtained from informed consent from the parents of the diseased children treated at Vision Research Foundation, Sankara Nethralaya and the protocol was approved by the Institutional Ethics Committee of Vision Research Foundation. We stored the tissues at −80 °C until further use.

Normal retina samples were collected from the healthy cadaveric eyes, post corneal transplantation supplied by C U Shah Eye Bank, Medical Research Foundation, Sankara Nethralaya. This study was conducted at Vision Research Foundation, Sankara Nethralaya, India, and was approved by the Vision Research Foundation Institutional Ethics Board (Ethical clearance no: 249B-2011-P).

RNA extraction for RNA-seq

RNA was extracted from tumors and normal retina using TRIzol reagent (#15596026, Thermo Fisher Scientific, Waltham, MA, USA) according to manufacturer's protocol. The quality and concentration of RNA were determined on 2200 TapeStation using the RNA-specific Tapes and reagents (#5067-5576, 5577, Agilent Technologies, Santa

Clara, CA, USA) and Qubit 3.0 Fluorimeter (#Q33216, Thermo Fisher Scientific) with RNA HS Assay (#Q32852, Thermo Fisher Scientific).

RNA library preparation and RNA-seq

After the RNA passed the defined quality control measures, the library was prepared using the TruSeq RNA Library Prep Kit V2 (#RS-122-2001/RS-122-2002, Illumina Inc., San Diego, CA, USA). Using divalent cations under high temperature, the Ribo-depleted RNA was fragmented. Initially, the first-strand cDNA was developed from fragmented RNA by using reverse transcriptase and random primers, followed by second-strand cDNA synthesis using DNA polymerase I and RNase H. A single 'A' base was added, and cDNA was then ligated to the adapters. This product was purified and amplified using PCR to make the final cDNA library. This library was quantified using Qubit DNA Assay and by using DNATapeStation D1000 Screen Tape (#5067-5582,5583, Agilent Technologies) amplified and sequenced on the HiSeq2500 with 100 bp paired-end chemistry. The TruSeq Universal Adapter is 5′AATGATACGGCGACCACCGAGATC TACACTCTTTCCCTACACGACGCTCTTCCGATCT3′.T and the TruSeq Illumina Index Adapter is as follows: 5′GA TCGGAAGAGCACACGTCTGAACTCCAGTCAC [IND EX] ATCTCGTATGCCGTCTTCTGCTTG3′. This was performed at Medgenome labs, Bangalore.

Bioinformatics

The raw fastq files generated during sequencing were first subjected to quality check to filter out substandard data. This was followed by adapter trimming, which was done using CUTADAPT v-1.8dev (ftp://ftp.ensembl.org/pub/release 75/gtf/homo_sapiens/Homo_sapiens.GRCh37). The processed data had no contamination from non-polyA tailed RNAs, mitochondrial genome sequences, ribosomal RNAs, transfer RNAs, adapter sequences due to the usage of BOWTIE2 v-2.2.4 [31]. The paired-end reads were aligned to reference human genome, GRCh37/hg19 using HISAT v-0.1.7 [32]. The gene expression in normal retina and RB tumors were calculated using FPKM values (Fragments Per Kilobase of transcript per Million mapped reads) using CUFFLINKS v-2.2.1 [33]. Significant differences in the FPKM values for the seven tumors and three retina sample genes were calculated by performing DESeq analysis [34]. DESeq2 was used to get the Differential Gene Expression for RNA-SEQ experiment. This used negative binomial distribution model to calculate the differential expression of the genes and was run on R script. The raw counts represented as a matrix were used as the input for DESeq2. For each sample, the number of sequences, which have been assigned to each gene, was reported. The values in the matrix were un-normalized counts. Deseq2 normalization was based on the retina ($N = 3$) and retinoblastoma samples ($N = 7$) as control and test samples. Prefiltering was done by removing reads with low reads to reduce the data size. The technical replicates were collapsed by combining the counts from technical replicates into single columns of the count matrix. The term *technical replicate* implies multiple sequencing runs of the same library. The output of DESeq2 consisted of the Ensembl gene ID, base mean, log2 fold change-retinoblastoma versus retina, standard error (IfcSE), stat—Wald statistic, *P* value —Wald test *P* value and adjusted *P* values. We used adjusted *P* values for obtaining significant fold change between the retinoblastoma and retina samples. A distribution of these log2 (fold change) values was found to be normally distributed. Those genes which were found to have $-2 \leq \log2$ (fold change) ≥ 2 were considered statistically significant.

Building metabolic models

Top–down approach was used to generate the metabolic models from the normal healthy retina and RB patient data. Currently, many variants of the model building algorithms are available, that is, GIMME [35], iMAT [36], FastCore [37], MBA [38], etc., and herein, we considered iMAT/Shlomi for model building. Threshold for gene expression, that is, > 1.5 is usually considered [39,40]. A user-defined threshold of 2 was chosen, such that genes that have an expression value ≥ 2 were considered to be associated with a primary reaction set. The primary reaction set represents reactions with high confidence level to be present in the cell type. We then compared the performance level of the first three algorithms for model building. For sample 1, 3382 reactions formed the primary reaction set, and GIMME captured 66% (2221/3382 reactions), iMAT captured 73% (2466/3382 reactions), and FastCore captured 6% (209/3382 reactions). Clearly iMAT captured the highest number of primary reactions in the model, as compared to GIMME and FastCore. The major reason for this discrepancy lies in the way the algorithm works for generating a draft model. While GIMME optimizes any given function (e.g., biomass reaction), making minimum addition to accomplish a non-zero flux through the defined objective, FastCore aims for flux consistency. iMAT works best for capturing reactions/pathways associated with the given data input. This is particularly handy for cases where a single objective is not obeyed/maintained, for example, mammalian cells.

The RNAseq data for the three healthy samples were summed up, and a cumulative expression value was considered to represent a single healthy case. Additionally, if a gene is expressed across all the three healthy samples, it is assumed to be present in the combined model that represents the healthy case. This made the comparison to the cancer cases simpler. A data matrix was constructed, using the above threshold. This matrix had index values as 0, 1, and 2, wherein, 0 signifies expression value not meeting the threshold and 1 agreeing with the threshold. An index of 2 was assigned to those with very high expression (i.e., ≥ 100). This

matrix is the first-step input for iMAT algorithm. The gap filling was then done using MILP (mixed integer linear programming) approach, maintaining the defined stoichiometric and thermodynamic constraints [36]. The MBA algorithm [38] also uses MILP to generate context-specific models and relies on multiple tissue-specific molecular data. However, model accuracy levels have been shown to be similar for iMAT and MBA [41]. Additionally, iMAT ensured maximum addition of reactions corresponding to highly expressed genes, which were further expected to carry active metabolic flux. At this stage, the models were termed as draft models that required further curation for its reaction and metabolite contents, in order to abide the sanity checks as well as capture true retina biochemistry (described below).

Model curation using literature data

Once the eight draft models (i.e., one model capturing combined healthy data and seven RB RNAseq data) were generated, sanity checks were performed to test the predictive capacity. These tests include (a) non-zero flux through maintenance and biomass reactions, (b) model curation to resolve network gaps, and (c) checks for mass balance. Healthy retina cells do not replicate [42]; while the addition of biomass reaction to the combined healthy draft model, the deoxynucleotide-triphosphates were removed, and a biomass maintenance reaction was added. This ensured that the healthy model performs only maintenance functions, rather than cellular duplication. Contrastingly, the draft models for RB were added with the biomass reactions as in Recon 2 [17].

Model validation

Retina function tests

Extensive manual curation of relevant scientific literature was done to formulate 53 metabolic objectives representing the general and unique biochemical functionalities of the retina. Additionally, two negative controls were set up representing the metabolic function that cannot be accomplished by retina alone (see Doc S1 for details). Flux balance analysis [43] (FBA) was used to optimize one function at a time. FBA assumes a steady state, wherein, the sum of the input flux equals the sum of the output flux. This follows as, $dx/dt = 0$, that is, the change in concentration of metabolites over time is zero. The mass balance for FBA is given as, $S \cdot v = 0$. S is the stoichiometric matrix formed by $m \times n$ (m are the metabolites occupying the row space, and n are the reactions in the column space of S). v is the flux vector for each reaction in the network, hence, is of size $n \times 1$. FBA optimizes an objective using linear programming, under the given constraints. Optimizing one function at a time gives a clear understanding of the entire metabolic capacity of the cell. Similar tests have been performed both for global human metabolic network [18] as well as cell-specific network of small intestine [44].

Secretion profile

Metabolites known to be secreted by healthy and RB were checked in the secretion profiles of the respective models. FastFVA [45] was used to calculate the minimum and maximum flux through the exchange reactions to determine the secretion profile. Flux variability analysis uses FBA to maximize and minimize each network reaction under the set constraints.

All fluxes were computed and given in mmol·gDW^{-1} h^{-1}. All simulations were carried out with MATLAB (Mathworks, Inc., Natick, MA, USA) as programming environment, using TOMLAB (TomOpt Inc., Seattle, WA, USA) as a linear programming solver, and the COBRA toolbox [46].

LC-MS MS methods

Cells Rb−/− and Rb +/+ were washed in 150 mM sodium chloride and the liquid removed before the cells were collected in 500 μL of chilled Acetonitrile/methanol/water (40/40/20) (Sigma, St. Louis, MO, USA, ACS grade). The cells were then vortexed and placed on dry ice. Each pellet was frozen and thawed three times. These were then spun at 21 000 ***g*** for 10 min. The lysate was lyophilized and frozen in liquid nitrogen. Before analysis, the samples were resuspended in 20 μL of HPLC water. The LC-MS/MS analysis was done as described in [47]. Briefly, analysis was performed on a 5500 QTRAP hybrid triple quadrupole mass spectrometer (AB/SCIEX, Framingham, MA, USA) coupled to a Prominence UFLC HPLC system (Shimadzu, Kyoto, Japan). 10 μL pools of metabolites were injected and analyzed using selected reaction monitoring (SRM) for 258 water-soluble metabolites. Ions were made using an ESI voltage of +4900 V in (+) ion mode and −4500 V in (−) ion mode. Data points were collected per detected metabolite using a dwell time of 3 ms per SRM transition and a total cycle time of 1.55 s. Delivery to the mass spectrometer was completed under normal phase chromatography conditions using a 4.6 mm i.d × 10 cm Amide Xbridge HILIC column (Waters Corp, Milford, MA, USA) at 300 mL·min^{-1}. Gradients were measured starting from 85% buffer B (HPLC grade acetonitrile) to 42% B from 0 to 5 min; 42% B to 0% B from 5 to 16 min; 0% B was held from 16 to 24 min; 0% B to 85% B from 24 to 25 min; 85% B was held for 7 min to re-equilibrate the column. Buffer A was comprised of 20 mM ammonium hydroxide/20 mM ammonium acetate (pH = 9.0) in water : acetonitrile (95 : 5). Peak areas from the total ion current for each metabolite SRM transition were integrated using MULTIQUANT v2.0 software (AB/SCIEX).

Analysis of synthetic lethals

Fast-SL algorithm [48] was used to identify all possible synthetic lethals and reaction pairs in healthy retina and different RB metabolic networks. Additionally, we identified potential compensatory reaction pathways for each of the

synthetic lethals (O. Mohite & K. Raman, unpublished results) to understand how metabolic fluxes are rerouted when one reaction of a synthetic lethal pair is deleted.

Results and Discussion

In this study, we developed patient-specific metabolic models of healthy retina and RB using iMAT algorithm [36]. The algorithm integrated the RNAseq data from healthy and retinoblastoma patients onto the metabolic model. Additionally, the generated draft models were further manually curated to improve the model contents and predictions. COBRA modeling analysis methods were employed to identify the fundamental biochemical differences between the healthy versus RB models as well as metabolic hallmarks between different RB models. The model prediction with respect to the RB-specific metabolite secretion was confirmed using MS/MS of human retinal cells depleted of RB1. Finally, synthetic lethals for RB was predicted as potential drug targets (Fig. 1).

RNAseq data

The gene expression profiling of healthy and RB cells yielded 57 867 transcripts, which mapped to 23, 453 unique Entrez genes with their corresponding expression values (Table S1A). The differential gene expression analysis using DESeq algorithm exhibited significant fold changes in 16% genes ($P < 0.05$) among the unique Entrez genes (Table S1B).

When we considered only the metabolic genes satisfying the thresholds (as mentioned in methods section), for building the metabolic models using FPKM values, 2825 genes formed the latter category, that is, 84%. The most recent human metabolic network, Recon 2 [17], was used to derive subsequent metabolic models of both normal retina and RB. The mapped metabolic genes present in the RNAseq data (i.e., 1713 genes) represented 99% of the genetic content of Recon 2, making Recon 2 as an ideal choice for subsequent investigation.

Model statistics

The first draft models capturing data from the healthy and the RB datasets were curated for their reaction and metabolite content (Table S2). Since retina cells growing *in vivo* do not replicate [42], a 'biomass maintenance reaction' was added to the healthy model and tested for non-zero flux. Additionally, exchange reactions were added for all the metabolites present in the extracellular space of the draft models. This was not performed by the iMAT algorithm and had to be added manually to enable a functional model. Furthermore, phospholipid metabolism was absent in the draft model, hence, added as per evidence from corresponding literature [49]. This ensured high quality of the reaction content of the final model. Similarly, the draft RB models were added with Recon 2 biomass reaction and checked for a non-zero flux. As stated above, addition of exchange reactions further enabled active biomass in the RB models. Although there was not much improvement in resolving dead-ends in the draft models (Table S2), the final models definitely scored more for their final reaction content that enabled a functional biomass. The final network components of all the models are given in Table 1, for details follow Table S3.

Performance for retina function tests

In order to know the major metabolic differences between a healthy and cancerous retina, 55 retina functions tests were formulated and tested, Table 2. Of these, 49% (27/55) were found to be affected in RB. Interestingly, 70% (19/27) of affected functions were performed differently across the seven RB models (Fig. 2, Table S4).

Significant differences between healthy and cancer models

Overall, six of the RB models performed lowly in accomplishing higher flux through the retina function tests (Fig. 2). Surprisingly, the third RB model achieved 40% higher flux through synthesis of omega-3 essential fatty acids, that is, docosapentaenoic acid (C22:5) and docosahexaenoic acid (C22:6). Furthermore, flux through biomass reaction resulted in 6% increase in this particular RB model (Fig. 2). It has been previously established that very long-chain fatty acids play critical roles in cancer, that is, for membrane synthesis, resistance to oxidative stress, survival under energy stress, redox balance, proliferation, and invasion [50]. Furthermore, the proto-oncogene *RB1* mutation that causes retinoblastoma tumor has also been shown to be involved in deregulation of lipid metabolism [5]. The developed RB model, thus, captured this cellular reprogramming and found that these tumors preferentially use very long-chain fatty acid synthesis for its survival.

The second reaction of urea cycle, that is, ornithine transcarbamylase (GeneID: 5009, *OTC*, EC 2.1.3.3), has been shown to absent in normal retina [51]. Interestingly, the first reaction of the urea cycle, that is, mitochondrial carbamoyl phosphate synthetase 1 (GeneID: 1373, *CPS1*, EC 6.3.4.16) was found to be

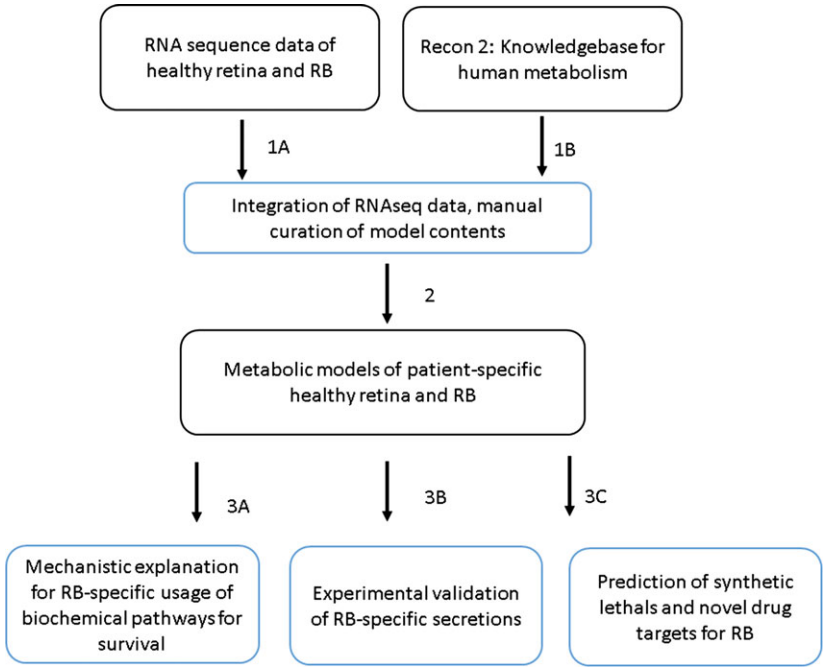

Fig. 1. Workflow followed in the present study. The RNA sequence data were used to build patient-specific metabolic models (1A). The model building algorithm, iMAT, was used to integrate the data and derive the metabolic models from the human metabolic network, Recon 2 [17] (1B). The models were further curated for their network components to derive functional models (2). The developed models were then used to explain the RB-specific metabolism (3A). The models secretion profile was validated *via* MS/MS experiments (3B), and potential drug targets predicted *via* synthetic lethal study (3C).

Table 1. Network contents of healthy and RB models, and their corresponding performance of retina function tests. Refer to Table S4 for details.

Models	Reactions	Unique metabolites	Blocked reactions	Unique genes	Tasks performed	Tasks affected
Combined healthy model	5287	2090	1050	1395	53	Non
RB model 1	4246	1911	1232	1195	48	18
RB model 2	4988	2053	1170	1280	49	13
RB model 3	5028	2062	1140	1248	51	14
RB model 4	4943	2045	1163	1216	51	10
RB model 5	4967	2044	1155	1270	47	12
RB model 6	5001	2057	1150	1304	48	13
RB model 7	4673	1978	1205	1215	44	18

absent across all the seven RB models, hence, the inactive or null flux (Fig. 2). However, the cytosolic version of CPS1 reaction was retained in the RB models to synthesize carbamoyl-asparate, *via* the aspartate carbamoyltransferase (GeneID: 790, *CAD*, EC 2.1.3.2), which is further utilized to derive orotate and uridine-based nucleotides for cellular duplication or biomass. This behavior was not seen in RB model 1, due to which we see a 47% lower flux through the corresponding biomass reaction (Fig. 2).

The amino acid arginine is an important biomass precursor. Hence, the RB models conserves it *via* reducing the flux through the arginase reaction (GeneID: 383, 384, *ARG1*, *ARG2*, EC 3.5.3.1), by 99% on an average, Fig. 2. The arginine is then used to synthesize guanidinoacetate (*via* glycine amidinotransferase, GeneID: 2628, *GATM*, EC 2.1.4.1), a precursor for phosphocreatine. Phosphocreatine is then used for ATP or energy synthesis, favoring RB model growth. Consequently, the flux through argininosucinate synthetase (GeneID: 445, *ASS1*, EC 6.3.4.5) and argininosuccinase (GeneID: 435, *ASL*, EC 4.3.2.1) also drops to conserve arginine, by 88% on an average, across all the seven cancer models. Accordingly, several reports have been published

Table 2. Presence and absence of metabolic pathways in retina as per literature. Refer to Table S4 for details.

Metabolic pathway involved	Reaction name, objective in the model	Significance in retina with references
Phospholipid biosynthesis	Choline kinase (EC 2.7.1.32), CHOLK CTP:phosphocholine cytidyltransferase (EC 2.7.7.15), CHLPCTD Phosphoethanolamine cytidyltransferase (EC 2.7.7.14), PETHCT	Weiss–Kennedy pathway exists for *de novo* biosynthesis of phospholipids within retina [49]. Lipids in retina aid in regulating the mobility, orientation, regeneration and stability of rhodopsin (i.e., the visual pigment), and thus, are important for proper functioning of the visual cycle [49]. The list of identified phospholipids in the retina is mentioned in Table S7
Ganglioside biosynthesis	UPD-glucose ceramide glucosyltransferase (EC 2.4.1.80), UGCG Neuraminidase (EC 3.2.1.18), SIAASEly	The enzymes that are involved in the activation of carbohydrate moieties and attaching them on to the growing glycolipid are present in retina [49]. The list of identified gangliosides in the retina is mentioned in Table S7
Sterol/isoprenoid biosynthesis	HMG-CoA reductase (EC 1.1.1.88, 1.1.1.34), HMGCOARc Mevalonate kinase (EC 2.7.1.36), MEVK1x Squalene epoxidase (EC 1.14.99.7), SQLEr Lanosterol synthase (EC 5.4.99.7), LNSTLSr delta7-Reductase 1 (EC 1.3.1.21), DHCR72r delta7-Reductase 2 (EC 1.3.1.21), DHCR71r delta24-Reductase 1 (EC 1.3.1.72), r0783 delta24-Reductase 2 (EC 1.3.1.72), r1380	In retina, the cholesterol biosynthesis is yet to be completely understood. Although the cell fractions gave cholesterol, higher percentage of lanosterol and squalene was found. *De novo* versus cholesterol transport to retinal cells is a topic of debate. For our study, we took the key rate limiting enzymes of the pathway to study the same in tumor [49,67,68]
Amino acid metabolism	Glutamate Decarboxylase (EC 4.1.1.15), GLUDC Gamma-aminobutyric acid transaminase (mitochondrial) (EC 2.6.19.4), ABTArm Aspartate transaminase (EC 2.6.1.1), ASPTA	GABA is a well-known neuromodulator in the retina. The distribution of the GABA-synthesizing enzymes varied among the retinal cell types; this results in differential modulation among the cells. Taurine is one of the most abundant amino acids in the ocular tissues including the retina. In the retina, taurine promotes photoreceptor development and functions as a cytoprotectant against stress. It is also speculated to be a neurotransmitter. Due to the high concentration of taurine in the eye, it is considered for the model [69–71]
Urea cycle	Ornithine transcarbamylase, irreversible (EC 2.1.3.3), OCBTm Carbamoyl-phosphate synthase 1 (EC 6.3.4.16), CBPSam Argininosuccinate synthase (EC 6.3.4.5), ARGSS Argininosuccinase (EC 4.3.2.1), ARGSL Arginase (EC 3.5.3.1), ARGN Ornithine delta-aminotransferase (EC 2.6.1.13), ORNTArm	Completely functional urea cycle is not present in retina, as the enzyme ornithine transcarbamylase (EC 2.1.3.3) is absent. The identified enzymes of the retina also play a role in the biosynthesis of arginine, proline, and glutamate. Urea cycle and its related pathways are known to play a crucial role in many diseases of the eye and also cancer [51,62]
Glutathione metabolism	Glutathione reductase 1 (EC 1.8.1.7), GTHO Glutathione oxidoreductase mitochondria (EC 1.8.1.7), GTHOm Gamma-glutamylcysteine synthetase (EC 6.3.2.2), GLUCYS Glutathione peroxidase (EC 1.11.1.9), GTHP	Glutathione present in the retina and other ocular cells function as antioxidants and electron donor for peroxidases. The distribution of the enzymes related to its synthesis and catalysis is distributed mainly in the regions having high oxidation. Glutathione-s-transferase (EC 2.5.1.18) binds glutathione with xenobiotics and glutathione

Table 2. (Continued).

Metabolic pathway involved	Reaction name, objective in the model	Significance in retina with references
		peroxidase (EC 1.11.1.9) detoxifies. Glutathione is very important in retina and in cancer conditions; hence, it is considered for the study [72–76]
ROS defense	Catalase (EC 1.11.1.6), CATm Superoxide dismutase (EC 1.15.1.1), SPODM	Catalase (EC 1.11.1.6) and superoxide dismutase (EC 1.15.1.1) are involved in antioxdation of reactive oxygen species in the retinal cells. Defective antioxidation metabolism leads to accumulation of reactive oxygen species which leads to deleterious effects and thereby causes mutations and cell instability. This is the reason for considering the enzymes in the modeling [77–79]
Retinoid cycle	Lecithin retinol acyltransferase (11-cis), LRAT1 Retinol dehydrogenase (all-trans) (EC 1.1.1. 105), RDH1 Retinol dehydrogenase (all-trans, NADPH) (EC 1.1.1.105), RDH1a Retinol dehydrogenase (11-cis, NADPH) (EC 1.1.1.105), RDH3a Retinoid isomerase 1 (11-cis) (EC 5.2.1.7), RETI1 Retinoid isomerase 2 (EC 5.2.1.7), RETI3	Retinoid cycle is responsible for the conversion of 11-trans retinol to 11-cis retinal, which is indispensable in the vision cycle occurring in the photoreceptors and retinal pigment epithelium of the retina. LRAT1 is also involved with vitamin A metabolism; RDH1 has multiple isoforms which catalyze the conversion of retinol to reinal. The relevance of these enzymes in the retina and the associated cancer is absolute [80]
Fatty acid synthesis	Synthesis of tetradecanoic acid, sink_tdcoa[c] Synthesis of palmitic acid, sink_pmtcoa[c] Synthesis of stearate, sink_stcoa[c] Synthesis of arachidonate, sink_arachcoa[c] Synthesis of hexadecenoic acid, sink_hdcoa[c] Synthesis of octadecenoic acid, sink_odecoa [c] Synthesis of octadecadienoic acid, sink_lnlccoa[c] Synthesis of eicosenoic acid, sink_CE5151[c] Synthesis of icosatetraenoic acid, sink_arachdcoa[c] Synthesis of adrenic acid, sink_adrncoa[c] Synthesis of docosapentaenoic acid, sink_clpndcoa[c] Synthesis of cervoniv acid, sink_c226coa[c]	Fatty acids found in the dog and bovine retinal cells are majorly saturated fatty acids (80%) and polyunsaturated fatty acids (20%). Among the unsaturated fatty acids, the most abundant are 20:4n-3 and 22:6n-3. Fatty acids are key in lipid biosynthesis, which are in turn strategic in diseases like cancer [49]
Biomass	Biomass_reaction_modified	Maintenance function in healthy retina model. Replication in retinoblastoma models [42]
Purine biosynthesis	Synthesis of cyclic AMP (EC 4.6.1.1), ADNCYC Synthesis of cyclic GMP (EC 4.6.1.2), GUACYC	The ratio of cyclic GMP to cyclic AMP was almost uniform between the different regions of the retina and it is not uniform in the pigmented epithelium. Retina is a complex tissue with multiple cell type, whereas pigmented epithelium is a tissue with similar cell type. The disparity in metabolite composition between the tissues of the eye in normal state creates curiosity to understand the metabolism that drives these reactions [81]

Table 2. (Continued).

Metabolic pathway involved	Reaction name, objective in the model	Significance in retina with references
Folate biosynthesis	Synthesis of tetra-hydro-folate (EC 1.5.1.6), FTHFDH Synthesis of folate (EC 1.5.1.3), DHFR	10-Formyltetrahydrofolate dehydrogenase which is commonly found in liver is reported in retinal cells. Also, this holds significance toward the folate metabolism in the retina [82]
Glycine biosynthesis	Synthesis of glycine (EC 2.1.2.1), GHMT2rm	Localization of the three inhibitory neurotransmitters—Glycine, GABA, and glutamate—was seen in different cell types of the retina. Colocalization of the metabolites may hold connection to regulation of cellular activity and synthesis of one metabolite from the other (such as GABA from glutamate) [83]
Melatonin pathway	Synthesis of melatonin (EC 2.1.1.4), ACSRTNMT	Melatonin required by the retina and is derived from the pineal gland, as Hydroxyindole-O-methyltransferase was found to be absent in the human retina [84]
Pteridine biosynthesis	Synthesis of methylenetetrahydrofolate, DHPR2 Synthesis of tetrahydrobiopterin (EC 1.6.99.7), DHPR	Pteridine pathway byproducts are known to protect the tissues of the eye from light-induced oxidation, along with giving color to the lens. The localization of the enzymes synthesizing pteridine was identified in retina. Tetrahydropteridine, a product of this pathway, is a cofactor for tyrosine and tryptophan hydroxylase [85]

stating that arginosuccinate synthetase and arginosuccinase enzymes found to be differentially expressed and somatically silenced in cancer [52–54]. Furthermore, arginine deprivation and inhibition of urea cycle and arginine biosynthesis have been suggested as potential cancer treatment strategies [55,56]. In the current study, the generated RB models selectively use arginine for cellular energy. Thus, metabolic modeling can be successfully used to explain the underlying biochemical mechanisms of cancer cell survival.

Cholesterol is an important constituent of retinal lipid, accounting for about 2% of the dry weight of retina [49]. The RB models on an average had 47% lower flux through reactions of cholesterol synthesis pathway (Fig. 2). Consequently, operating cholesterol synthesis reactions at a lower rate preserved the important intermediate, that is, 'nadph' for utilization by other pathways. This was particularly true for RB model 3, wherein, the model had higher flux through 'nadph' utilizing reactions, including the fatty acid elongation, alpha and omega oxidation, cortisol, testosterone, leukotriene synthesis, and peroxisomal beta oxidation pathways, as compared to the healthy model. In line with this, enzymes of cholesterol metabolism have been suggested as potential targets for different tumors [57,58].

Significant differences between the RB models

Although the RB models exhibit different biochemical behaviors for a large number of metabolic pathways (Fig. 2), we next cover those of greatest significance.

Gamma-aminobutyric acid transaminase

Gamma-aminobutyric acid (GABA) is an important neurotransmitter for retinal neurons [59] and confers neurotrophic effects that aid retinal maturation and development [60]. There exists multiple alternative biosynthetic pathways for GABA, for example, aminobutyraldehyde dehydrogenase (GeneID; 223, *ALDH9A*, 1 EC 1.2.1.19), GABA transaminase (Gene ID: 18, *ABAT*, EC 2.6.1.19), or glutamate decarboxylase (Gene ID: 2571, *GAD1*, EC 4.1.1.15). All the RB models run either all of these or different combination of reactions to generate endogenous GABA. Consequently, the dehydrogenase reaction is absent in RB model 1, which is compensated by running the transaminase and decarboxylase reactions. Similarly, RB model 6 lacks the decarboxylase but utilizes alternative pathways. In contrast, RB models 2, 3, 4, 5, and 7 run all the above reactions. Interestingly, GABA has been shown to be involved in cancer cell metastasis

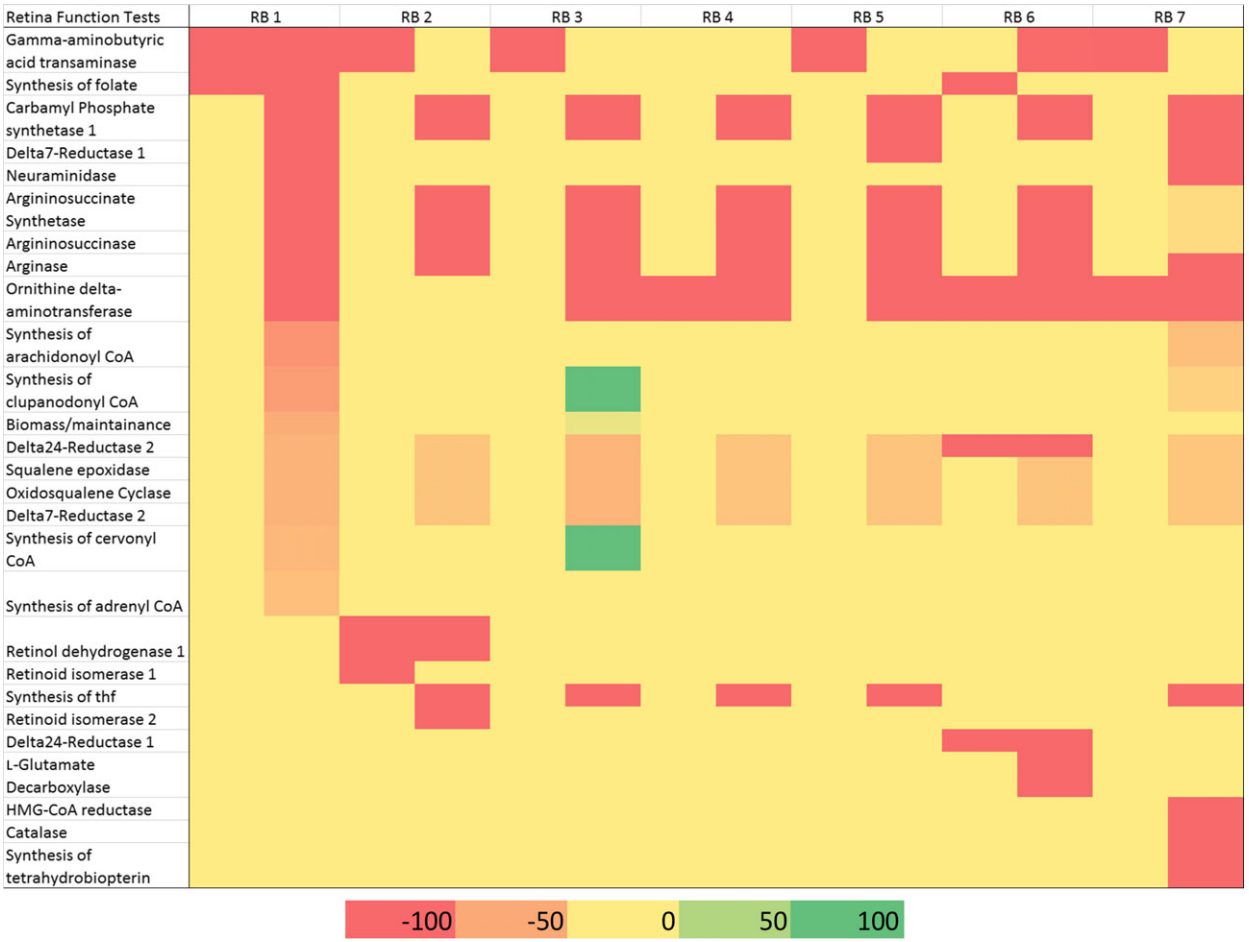

Fig. 2. Summary of retina function test results. Shown is the comparison of flux values of RB models to healthy model. Yellow color represents a value of zero, that is, no change between healthy and RB models. Red and green color represent percent decrease and increase, respectively.

and proliferation [61], and its high concentration has been found in various retinoblastomas [14].

Additionally, the reversible GABA transaminase is operated for synthesis of glutamate and succinate semialdehyde by RB models 2, 3, 5, and 7. Succinate semialdehyde is further converted to succinate, which is driven toward ATP synthesis, *via* the TCA cycle. Consequently, elevated glutamate levels have also been reported in retinoblastomas and other cancers [14].

While the RB model 4 runs GABA transaminase in either direction, the RB model 6 runs it majorly for GABA and alpha-keto-glutarate synthesis, wherein, the latter serves energy purpose of the cell.

Ornithine delta-aminotransferase

Ornithine transaminase (Gene ID: 4942, *OAT*, EC 2.6.1.13) is an important enzyme for retinal function. Being at the cross roads of glutamate metabolism, this enzyme is required for synthesis of glutamate from alpha-keto-glutarate, and glutamate 5-semialdehyde from ornithine, *via* transamination. The glutamate 5-semialdehyde is further utilized for proline synthesis. Deficiency of this enzyme causes gyrate atrophy of the choroid and retina (OMIM: 258870) characterized with ornithine accumulation [62]. Interestingly, the RB models 1, 3, 5, and 6 utilized this reaction for synthesis of alpha-keto glutarate for energy resource. The high flux through ornithine synthesis was then compensated *via* lowering flux through other ornithine synthesis reaction, that is, arginase (GeneID: 383, 384, *ARG1*, *ARG2*, EC 3.5.3.1), Fig. 2.

Long-chain fatty acid synthesis

Polyunsaturated C22 fatty acids, that is, docosapentaenoic acid (C22:5) and docosahexaenoic acid (C22:6), are important retinal membrane lipids, contributing to about 80% of the total polyunsaturates

[49]. Other long-chain fatty acids include the arachidonic acid (C20:4) and adrenic acid (C22:4) that make up the membrane lipid composition. The RB model 1, on an average, had 50% lower flux through synthesis of the above-mentioned fatty acids, as compared to the healthy retina model. The RB model 7, however, on an average, had 27% reduced flux through synthesis of only C22:4 and C22:5 fatty acids. Chain length of very long-chain fatty acids has been reported to be used for differentiating between cancer types [63]. Furthermore, metabolic profiling of retinoblastomas revealed that certain RB groups had increased lipids as compared to other RB groups that exhibited very low lipid concentrations [14]. Consequently, in our profile, RB model 3 had higher flux through very long-fatty acid synthesis (as mentioned above), while RB model 1 and 7 had lower flux.

Biomass

The notable difference in biomass flux was observed for RB models 1 and 3, wherein the former had 47% lower flux and the latter had 6% higher flux, respectively.

For other test functions mentioned in Fig. 2, 'Neuraminidase' and 'Retinoid isomerase 2' were absent in the concerned cancer models, resulting in null flux through these reactions as compared to the healthy retina model.

Comparison of secretion profile

Metabolic differences between the RB and healthy models were further identified based on their secretion profile. On an average, 74% of exchanges were active across the seven RB models, which were compared to the active exchanges in the healthy model, that is, 80%, Table 3. Follow Table S5 for details.

Table 3. Active metabolic secretion profile of healthy and RB models, and corresponding support from MS/MS experiments performed in the study and literature support gathered *via* manual curation of scientific literature. Refer to Table S5 for details.

Metabolic network	No. of active exchanges (% when compared to total model exchanges)	No. of active exchanges different from healthy (%)	% supported by MS/MS or literature
Healthy retina	429 (80)	458 (18) compared to RB average	20
RB 1	358 (83)	148 (41)	20
RB 2	371 (74)	72 (19)	22
RB 3	370 (75)	100 (27)	21
RB 4	371 (74)	85 (23)	22
RB 5	376 (75)	99 (26)	22
RB 6	385 (76)	81 (21)	21
RB 7	362 (73)	110 (30)	22

While 22 metabolites were found to be unique to the RB model, and absent in the healthy model, 208 metabolites were found to be shared between healthy and seven RB models, but with distinct flux value (Fig. 3). The latter set of metabolites was further explored with respect to their secretion pattern and involvement in core metabolic pathways. A majority of the metabolites were found to have a reduced secretion pattern (Fig. 3). Furthermore, the lipid and amino acid class of metabolites were the top scorers, where in, the flux values were either reduced or increased through their secretion reactions in RB models, as compared to healthy model (Fig. 3).

The active secretion profile of healthy and RB models was then evaluated for experimental support. While 20% of healthy secretion metabolites were supported *via* either experimental validation or literature curation, 22% of RB model metabolites were validated (Table S5). This discrepancy was mainly seen as much of the evidence was found for nucleotides (32%) and amino acid (28%) class of metabolites. However, in the current study, majority of the model predictions with respect to secretion profile was for lipid class (i.e., 38%, Fig. 3). Furthermore, a recent study done on mouse embryonic fibroblast cells also identified that upon knockdown of RB gene resulted in significant changes of cellular lipid composition [64]. Herein, we would like to emphasize on the need for targeted lipidomics experimentation for identification and validation of RB-specific metabolites that could aid in rapid medical diagnostics.

Synthetic lethals and metabolic rerouting analysis

The different RB models show difference in the number of synthetic lethals between them and also when compared to the "healthy model" (Fig. 4). RB1 contributed the highest number of single (19%) and double (26%) lethals to the total set. Healthy retina model had the lowest numbers, that is, 6% of single and 5% of double lethals of the total. This signifies the robustness of the healthy retina model as compared to the RB models, making the latter group amenable for predicting potential drug targets for curbing cellular biomass/duplication. In line with this, four single lethals and three double lethals were found to be common across all the eight models (Fig. 4), which highlight their essentiality for network robustness. However, RB1 (34 reaction pairs), RB3 (19

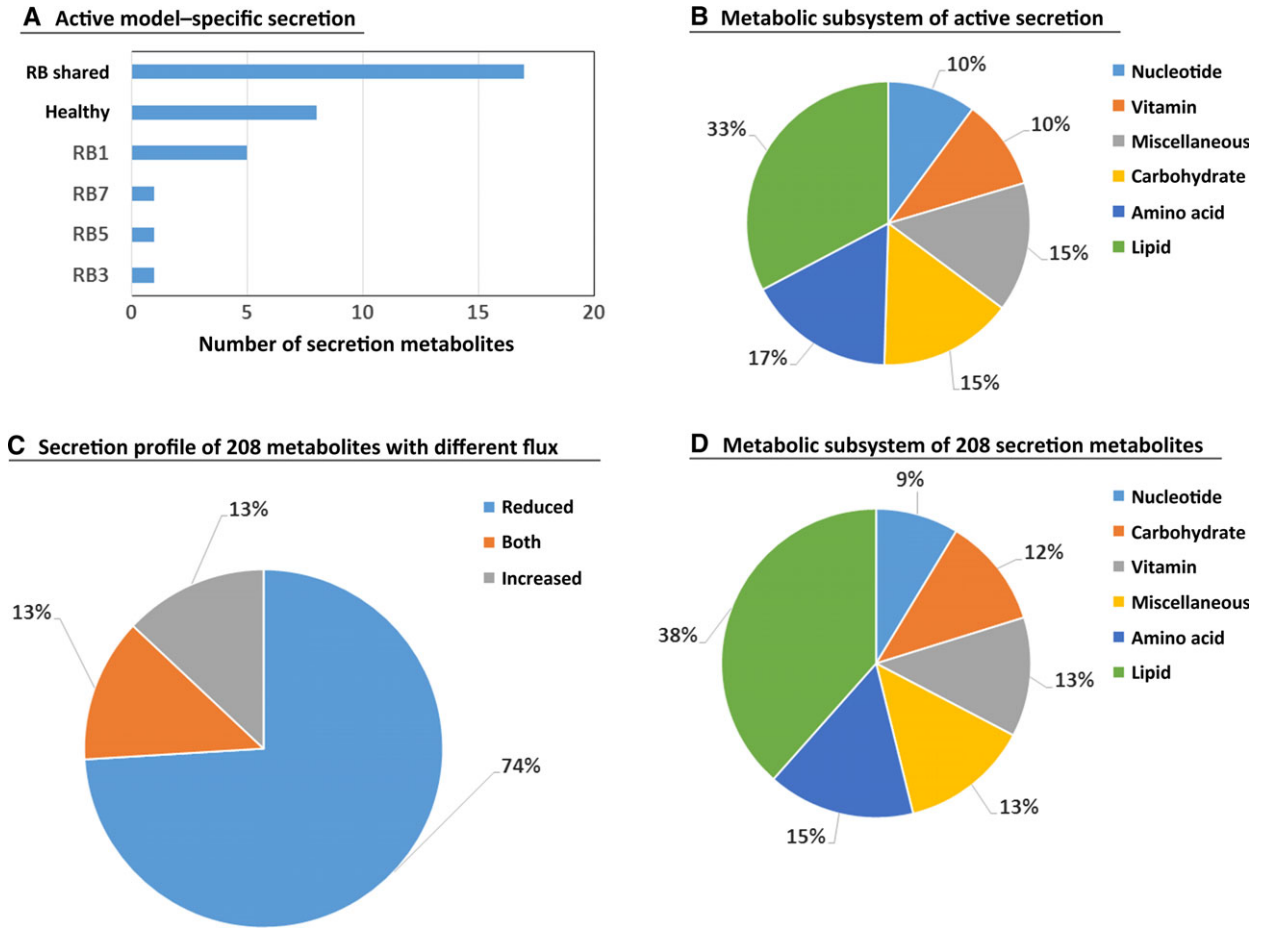

Fig. 3. Secretion profile comparison between healthy and cancer models and between the seven cancer models. (A) Exchange metabolites that are specific to the cancer models and absent in the healthy model. (B–D) Exchange metabolites common between the healthy and cancer models, with different secretion flux rate, which are common across the cancer models (B), highest number of metabolites were found to have a reduced flux value as compared to the healthy model (C), metabolic classification of the shared secretion metabolites (D).

reaction pairs), RB5 (12 reactions pairs), and RB7 (20 reaction pairs) models contained the maximum number of double lethal interactions and highlight the potential of synthetic lethal predictions for identifying cancer subtypes (Fig. 4). Details of the synthetic lethal single reactions and double lethals (i.e., pairs) can be found in Table S6.

Next, we analyzed how the single and double lethals vary their lethality condition across the eight models. Of the total 223 reactions, 81 unique reactions were considered for this analysis, Table S6. Interestingly, 79% of these unique reactions (i.e., 64/81 in Table S6) were found to be non-essential in healthy model. However, these were single or double lethals in at least one of the RB models. Such reactions with higher lethality specific to only RB cells could be studied further for developing potential anticancer drug targets (Table 4).

We next focused on the 13 single lethal targets suggested by the models to be lethal only in RB but not in healthy. Interestingly, eight of these (i.e., 62%) were found to be either used as drug targets or as prognostic markers for various cancers (Table 4). Of the remaining five targets, four of which were transport reactions transporting nucleotides and lipids were found to be novel in the current study and need experimental testing. Nevertheless, the potential of nucleoside transporter inhibitors for the treatment of ovarian cancer is already well established [65]. Therefore, we propose the use of lipid and nucleoside transporter inhibitors for retinoblastoma cases.

In order to classify predicted lethal interactions as double lethals, the basis of their precise reaction paring

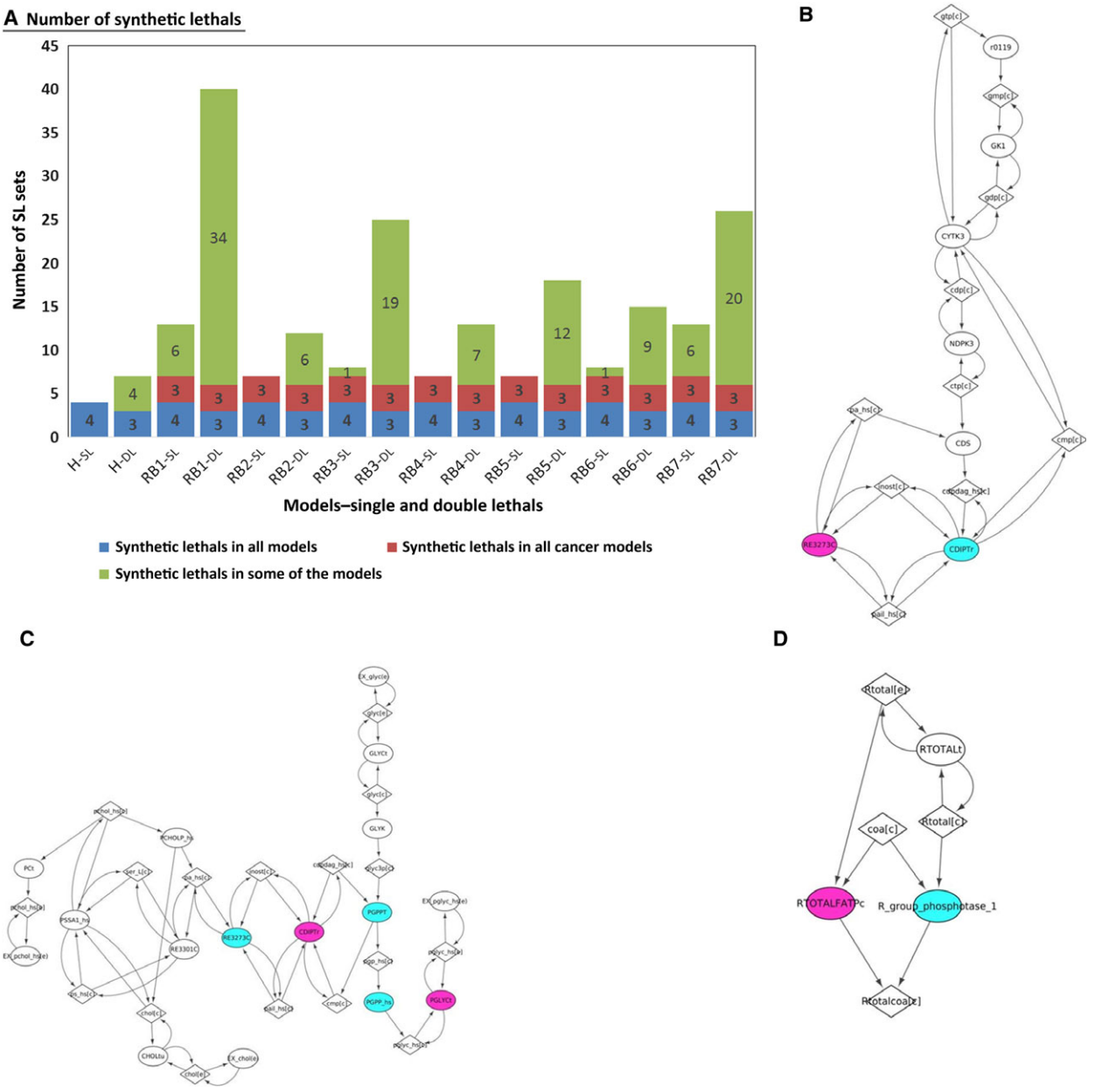

Fig. 4. Summary of synthetic lethals observed in the healthy and RB models. (A) Synthetic lethals (both single and double lethals) have been identified for multiple retinoblastoma models. H—Healthy model, Ci—Cancer model number i, sl—number of single lethals, dl—number of double lethals. The colored bars suggest the overlap in synthetic lethals denoted by different colors. Blue—common to all, red—common in all cancer models, and green—specific to models. (B–D) Bipartite graphs representing reactions and metabolites in minimal rerouting sets for synthetic lethals. Diamond represents metabolites and reactions are noted by ellipses. Second panel shows seven reactions in rerouting of synthetic lethal pair CDIPTr and RE3273C. Third panel shows 16 reactions required for rerouting of fluxes from PGLYCt to PGPP_hs and PGPPT. The last panel shows three reactions in rerouting between R_group_phosphotase_1 and RTOTALFATP.

needs to be completely evaluated. Surprisingly, double lethals (very often) result not only due to knockdown of two reactions but also the entire chain of reactions needs to be shutdown. All possible sets of minimal reactions that are required for the rewiring of fluxes between synthetic lethals reaction pairs were identified (Table S6). Such rerouting analysis gives us a list of important reactions forming compensatory pathways corresponding to a particular synthetic lethal. Hence, all the compensatory pathways need to be considered during early cancer drug development. Visualization of few of the subnetworks with respect to synthetic

Table 4. List of reactions which are essential/single lethal in RB models but are not essential in healthy models. Refer to Table S6 for details.

Reaction abbreviation	Reaction name (EC number)	Status in healthy model	Single lethal in RB models	Supported *via* literature/novel as per current study
CDIPTr	Phosphatidylinositol synthase (EC 2.7.8.11)	Double Lethal	RB 1, RB 3, RB 7	The enzyme is overexpressed in oral cancer and is a proposed drug target [86]
GK1	Guanylate kinase (EC 2.7.4.8)	Double Lethal	RB 6	The protein is a good target for chemotherapeutic agents. Additionally, upon fusion with other proteins, aids in killing cancer cells [87]
AGPAT1	1-acylglycerol-3-phosphate O-acyltransferase 1 (EC 2.3.1.51)	Nonlethal	RB 7	Acts as a cancer marker and proposed target for ovarian cancer [88,89], non-Hodgkin's lymphomas [90], endometrial tumor [91], and other tumors [92,93]
DTMPK	dTMP kinase (EC 2.7.4.12, 2.7.4.13, 2.7.4.9)	Nonlethal	RB 7	Thymidylate kinase in combination with doxorubicin can kill colon cancer cells regardless of p53 status [94]
GPAM_hs	Glycerol-3-phosphate acyltransferase (EC 2.3.1.15)	Nonlethal	RB 7	Suggested as a prognostic marker and a therapeutic target for breast cancer [95] and ovarian cancer [96]
PUNP6	Purine-nucleoside phosphorylase (Deoxyinosine) (EC 2.4.2.1, 2.4.2.4)	Nonlethal	RB 1	Analogs suggested to be of potential for cancer treatment [97]
LYStiDF	L-lysine transport *via* diffusion (extracellular to cytosol) (GeneID: 6542, 6541, 55089, 84889)	Nonlethal	RB 1	Lysine transporter, CAT-1 (GeneID: 6541) is overexpressed in colorectal cancer [98]. Additionally, suggested target for breast cancer. Its knockdown showed reduced cell survival [99]
DINt	Deoxyinosine transport *via* diffusion (GeneID: 3177)	Nonlethal	RB 1	Nucleoside transport proteins (ENT2) widely expressed in cancer, and suggested as prognostic marker for ovarian cancer [65,100]
Novel predictions in the present study				
DATPtn, DCTPtn, DGTPtn	dATP, dCTP, dGTP diffusion in nucleus	Nonlethal	All RB models	
PGLYCt	Phosphatidylglycerol transport	Double Lethal	RB 1, RB 7	
CDS	Phosphatidate cytidylyltransferase (EC 2.7.7.41)	Nonlethal	RB 1, RB 7	

lethals in healthy retina model was done using Cytoscape [66] (Fig. 4).

Conclusions

The present study used a constraint-based metabolic modeling approach for explaining the various biochemical phenomenon adopted by RB models for survival. These include preferential usage of arginine, GABA, glutamate, and ornithine metabolism for deriving cellular energy. Additionally, there is underutilization of cholesterol for preserving redox potential, that is, nadph. Furthermore, it is computationally reconfirmed that synthesis of long-chain/very long-chain fatty

acids can be used for identification of RB types. The current study also utilizes experimental data from RB-specific metabolic secretion profiles with respect to amino acid and nucleosides and proposes novel lipid class of metabolites. Single synthetic lethals that hold potential for developing novel drug targets for RB have been proposed for lipid and nucleoside transport proteins. Hence, given large-scale experimental validation of the model predictions, the present work could substantiate novel dimension for cancer research.

Acknowledgements

This work was supported by DST-INSPIRE Faculty award, Department of Science and Technology, India (DST/INSPIRE/04/2015/000036) to SS, and Department of Biotechnology, India Programme support for Research on Retinoblastoma (BT/01/CEIB/11/V/16) to SK and SL, DST-SERB (EMR/2015/00607) to SL.

Author contributions

SS and SE conceived the idea and designed the experiments. SS and RKRK developed and curated the tumor and retina models. OM and KR performed the synthetic lethality study. VK, PR, KSu, and SG handled the tissue samples. KSi performed the bioinformatics on the RNAseq data. BN and WM performed Mass spectroscopy. SS, SE, and RKRK wrote the manuscript.

References

1 Winkler BS (1983) The intermediary metabolism of the retina: biochemical and functional aspects. American Academy of Ophthalmology, San Francisco, CA.
2 Knudson AG Jr (1971) Mutation and cancer: statistical study of retinoblastoma. *Proc Natl Acad Sci USA* **68**, 820–823.
3 Seregard S, Lundell G, Svedberg H and Kivela T (2004) Incidence of retinoblastoma from 1958 to 1998 in Northern Europe: advantages of birth cohort analysis. *Ophthalmology* **111**, 1228–1232.
4 Broaddus E, Topham A and Singh AD (2009) Incidence of retinoblastoma in the USA: 1975-2004. *Br J Ophthalmol* **93**, 21–23.
5 Dimaras H, Kimani K, Dimba EA, Gronsdahl P, White A, Chan HS and Gallie BL (2012) Retinoblastoma. *Lancet* **379**, 1436–1446.
6 Leander C, Fu LC, Pena A, Howard SC, Rodriguez-Galindo C, Wilimas JA, Ribeiro RC and Haik B (2007) Impact of an education program on late diagnosis of retinoblastoma in Honduras. *Pediatr Blood Cancer* **49**, 817–819.
7 Nyamori JM, Kimani K, Njuguna MW and Dimaras H (2012) The incidence and distribution of retinoblastoma in Kenya. *Br J Ophthalmol* **96**, 141–143.
8 Moll AC, Imhof SM, Bouter LM and Tan KE (1997) Second primary tumors in patients with retinoblastoma. A review of the literature. *Ophthalmic Genet* **18**, 27–34.
9 Shields CL, Kaliki S, Al-Dahmash S, Rojanaporn D, Leahey A, Griffin G, Jabbour P and Shields JA (2013) Management of advanced retinoblastoma with intravenous chemotherapy then intra-arterial chemotherapy as alternative to enucleation. *Retina* **33**, 2103–2109.
10 Ortiz MV and Dunkel IJ (2016) Retinoblastoma. *J Child Neurol* **31**, 227–236.
11 Lang P, Kim JW, McGovern K, Reid MW, Subramanian K, Murphree AL and Berry JL (2018) Porous orbital implant after enucleation in retinoblastoma patients: indications and complications. *Orbit*, 1–6. https://doi.org/10.1080/01676830.2018.1440605
12 Friedman DN, Chou JF, Oeffinger KC, Kleinerman RA, Ford JS, Sklar CA, Li Y, McCabe MS, Robison LL, Marr BP *et al.* (2016) Chronic medical conditions in adult survivors of retinoblastoma: results of the Retinoblastoma Survivor Study. *Cancer* **122**, 773–781.
13 Seth R, Singh A, Guru V, Chawla B, Pathy S and Sapra S (2017) Long-term follow-up of retinoblastoma survivors: experience from India. *South Asian J Cancer* **6**, 176–179.
14 Kohe S, Brundler MA, Jenkinson H, Parulekar M, Wilson M, Peet AC and McConville CM (2015) Metabolite profiling in retinoblastoma identifies novel clinicopathological subgroups. *Br J Cancer* **113**, 1216–1224.
15 Thiele I and Palsson BO (2010) A protocol for generating a high-quality genome-scale metabolic reconstruction. *Nat Protoc* **5**, 93–121.
16 Duarte NC, Becker SA, Jamshidi N, Thiele I, Mo ML, Vo TD, Srivas R and Palsson BO (2007) Global reconstruction of the human metabolic network based on genomic and bibliomic data. *Proc Natl Acad Sci USA* **104**, 1777–1782.
17 Thiele I, Swainston N, Fleming RM, Hoppe A, Sahoo S, Aurich MK, Haraldsdottir H, Mo ML, Rolfsson O, Stobbe MD *et al.* (2013) A community-driven global reconstruction of human metabolism. *Nat Biotechnol* **31**, 419–425.
18 Brunk E, Sahoo S, Zielinski DC, Altunkaya A, Dräger A, Mih N, Gatto F, Nilsson A, Preciat Gonzalez GA, Aurich MK *et al.* (2018) Recon3D enables a three-dimensional view of gene variation in human metabolism. *Nat Biotechnol* **36**, 272–281.
19 Aurich MK and Thiele I (2016) Computational modeling of human metabolism and its application to systems biomedicine. *Methods Mol Biol* **1386**, 253–281.

20 Bordbar A and Palsson BO (2011) Using the reconstructed genome-scale human metabolic network to study physiology and pathology. *J Intern Med* **271**, 131–141.
21 Yizhak K, Chaneton B, Gottlieb E and Ruppin E (2015) Modeling cancer metabolism on a genome scale. *Mol Syst Biol* **11**, 817.
22 Robaina Estevez S and Nikoloski Z (2014) Generalized framework for context-specific metabolic model extraction methods. *Front Plant Sci* **5**, 491.
23 Aurich MK, Fleming RMT and Thiele I (2017) A systems approach reveals distinct metabolic strategies among the NCI-60 cancer cell lines. *PLoS Comput Biol* **13**, e1005698.
24 Folger O, Jerby L, Frezza C, Gottlieb E, Ruppin E and Shlomi T (2011) Predicting selective drug targets in cancer through metabolic networks. *Mol Syst Biol* **7**, 501.
25 Lewis NE and Abdel-Haleem AM (2013) The evolution of genome-scale models of cancer metabolism. *Front Physiol* **4**, 237.
26 Kaelin WG Jr (2005) The concept of synthetic lethality in the context of anticancer therapy. *Nat Rev Cancer* **5**, 689–698.
27 Nijman SM (2011) Synthetic lethality: general principles, utility and detection using genetic screens in human cells. *FEBS Lett* **585**, 1–6.
28 O'Neil NJ, Bailey ML and Hieter P (2017) Synthetic lethality and cancer. *Nat Rev Genet* **18**, 613–623.
29 Apaolaza I, San Jose-Eneriz E, Tobalina L, Miranda E, Garate L, Agirre X, Prosper F and Planes FJ (2017) An in-silico approach to predict and exploit synthetic lethality in cancer metabolism. *Nat Commun* **8**, 459.
30 Frezza C, Zheng L, Folger O, Rajagopalan KN, MacKenzie ED, Jerby L, Micaroni M, Chaneton B, Adam J, Hedley A *et al.* (2011) Haem oxygenase is synthetically lethal with the tumour suppressor fumarate hydratase. *Nature* **477**, 225–228.
31 Langmead B and Salzberg SL (2012) Fast gapped-read alignment with Bowtie 2. *Nat Methods* **9**, 357–359.
32 Kim D, Langmead B and Salzberg SL (2015) HISAT: a fast spliced aligner with low memory requirements. *Nat Methods* **12**, 357–360.
33 Trapnell C, Roberts A, Goff L, Pertea G, Kim D, Kelley DR, Pimentel H, Salzberg SL, Rinn JL and Pachter L (2012) Differential gene and transcript expression analysis of RNA-seq experiments with TopHat and Cufflinks. *Nat Protoc* **7**, 562–578.
34 Anders S, McCarthy DJ, Chen Y, Okoniewski M, Smyth GK, Huber W and Robinson MD (2013) Count-based differential expression analysis of RNA sequencing data using R and Bioconductor. *Nat Protoc* **8**, 1765–1786.
35 Chang RL, Xie L, Bourne PE and Palsson BO (2010) Drug off-target effects predicted using structural analysis in the context of a metabolic network model. *PLoS Comput Biol* **6**, e1000938.
36 Shlomi T, Cabili MN, Herrgard MJ, Palsson BO and Ruppin E (2008) Network-based prediction of human tissue-specific metabolism. *Nat Biotechnol* **26**, 1003–1010.
37 Vlassis N, Pacheco MP and Sauter T (2014) Fast reconstruction of compact context-specific metabolic network models. *PLoS Comput Biol* **10**, e1003424.
38 Jerby L, Shlomi T and Ruppin E (2010) Computational reconstruction of tissue-specific metabolic models: application to human liver metabolism. *Mol Syst Biol* **6**, 401.
39 Black MB, Parks BB, Pluta L, Chu TM, Allen BC, Wolfinger RD and Thomas RS (2014) Comparison of microarrays and RNA-seq for gene expression analyses of dose-response experiments. *Toxicol Sci* **137**, 385–403.
40 Andersen ME, Cruzan G, Black MB, Pendse SN, Dodd D, Bus JS, Sarang SS, Banton MI, Waites R and McMullen PD (2017) Assessing molecular initiating events (MIEs), key events (KEs) and modulating factors (MFs) for styrene responses in mouse lungs using whole genome gene expression profiling following 1-day and multi-week exposures. *Toxicol Appl Pharmacol* **335**, 28–40.
41 Opdam S, Richelle A, Kellman B, Li S, Zielinski DC and Lewis NE (2017) A systematic evaluation of methods for Tailoring Genome-Scale metabolic models. *Cell Syst* **4**, 318–329.e6.
42 Scammon RE and Armstrong EL (1925) On the growth of the human eyeball and optic nerve. *J Comp Neurol* **38**, 165–219.
43 Orth JD, Thiele I and Palsson BO (2010) What is flux balance analysis? *Nat Biotechnol* **28**, 245–248.
44 Sahoo S and Thiele I (2013) Predicting the impact of diet and enzymopathies on human small intestinal epithelial cells. *Hum Mol Genet* **22**, 2705–2722.
45 Gudmundsson S and Thiele I (2010) Computationally efficient flux variability analysis. *BMC Bioinformatics* **11**, 489.
46 Schellenberger J, Que R, Fleming RM, Thiele I, Orth JD, Feist AM, Zielinski DC, Bordbar A, Lewis NE, Rahmanian S *et al.* (2011) Quantitative prediction of cellular metabolism with constraint-based models: the COBRA Toolbox v2.0. *Nat Protoc* **6**, 1290–1307.
47 Nicolay BN, Gameiro PA, Tschöp K, Korenjak M, Heilmann AM, Asara JM, Stephanopoulos G, Iliopoulos O and Dyson NJ (2013) Loss of RBF1 changes glutamine catabolism. *Genes Dev* **27**, 182–196.
48 Pratapa A, Balachandran S and Raman K (2015) Fast-SL: an efficient algorithm to identify synthetic

lethal sets in metabolic networks. *Bioinformatics* **31**, 3299–3305.
49 Fliesler SJ and Anderson RE (1983) Chemistry and metabolism of lipids in the vertebrate retina. *Prog Lipid Res* **22**, 79–131.
50 Santos CR and Schulze A (2012) Lipid metabolism in cancer. *FEBS J* **279**, 2610–2623.
51 Rao GN and Cotlier E (1984) Urea cycle enzymes in retina, ciliary body-iris, lens and senile cataracts. *Exp Eye Res* **39**, 483–495.
52 Dillon BJ, Prieto VG, Curley SA, Ensor CM, Holtsberg FW, Bomalaski JS and Clark MA (2004) Incidence and distribution of argininosuccinate synthetase deficiency in human cancers: a method for identifying cancers sensitive to arginine deprivation. *Cancer* **100**, 826–833.
53 Nagamani SC and Erez A (2016) A metabolic link between the urea cycle and cancer cell proliferation. *Mol Cell Oncol* **3**, e1127314.
54 Delage B, Fennell DA, Nicholson L, McNeish I, Lemoine NR, Crook T and Szlosarek PW (2010) Arginine deprivation and argininosuccinate synthetase expression in the treatment of cancer. *Int J Cancer* **126**, 2762–2772.
55 Stasyk OV, Boretsky YR, Gonchar MV and Sibirny AA (2015) Recombinant arginine-degrading enzymes in metabolic anticancer therapy and bioanalytics. *Cell Biol Int* **39**, 246–252.
56 Wheatley DN (2004) Controlling cancer by restricting arginine availability–arginine-catabolizing enzymes as anticancer agents. *Anticancer Drugs* **15**, 825–833.
57 Brown DN, Caffa I, Cirmena G, Piras D, Garuti A, Gallo M, Alberti S, Nencioni A, Ballestrero A and Zoppoli G (2016) Squalene epoxidase is a bona fide oncogene by amplification with clinical relevance in breast cancer. *Sci Rep* **6**, 19435.
58 Maione F, Oliaro-Bosso S, Meda C, Di Nicolantonio F, Bussolino F, Balliano G, Viola F and Giraudo E (2015) The cholesterol biosynthesis enzyme oxidosqualene cyclase is a new target to impair tumour angiogenesis and metastasis dissemination. *Sci Rep* **5**, 9054.
59 Bui BV, Hu RG, Acosta ML, Donaldson P, Vingrys AJ and Kalloniatis M (2009) Glutamate metabolic pathways and retinal function. *J Neurochem* **111**, 589–599.
60 Lake N (1994) Taurine and GABA in the rat retina during postnatal development. *Vis Neurosci* **11**, 253–260.
61 Young SZ and Bordey A (2009) GABA's control of stem and cancer cell proliferation in adult neural and peripheral niches. *Physiology (Bethesda)* **24**, 171–185.
62 Rao GN and Cotlier E (1984) Ornithine delta-aminotransferase activity in retina and other tissues. *Neurochem Res* **9**, 555–562.
63 Yamashita Y, Nishiumi S, Kono S, Takao S, Azuma T and Yoshida M (2017) Differences in elongation of very long chain fatty acids and fatty acid metabolism between triple-negative and hormone receptor-positive breast cancer. *BMC Cancer* **17**, 589.
64 Muranaka H, Hayashi A, Minami K, Kitajima S, Kohno S, Nishimoto Y, Nagatani N, Suzuki M, Kulathunga LAN, Sasaki N *et al.* (2017) A distinct function of the retinoblastoma protein in the control of lipid composition identified by lipidomic profiling. *Oncogenesis* **6**, e350.
65 Farre X, Guillén-Gómez E, Sánchez L, Hardisson D, Plaza Y, Lloberas J, Casado FJ, Palacios J and Pastor-Anglada M (2004) Expression of the nucleoside-derived drug transporters hCNT1, hENT1 and hENT2 in gynecologic tumors. *Int J Cancer* **112**, 959–966.
66 Shannon P, Markiel A, Ozier O, Baliga NS, Wang JT, Ramage D, Amin N, Schwikowski B and Ideker T (2003) Cytoscape: a software environment for integrated models of biomolecular interaction networks. *Genome Res* **13**, 2498–2504.
67 Fliesler SJ and Keller RK (1997) Isoprenoid metabolism in the vertebrate retina. *Int J Biochem Cell Biol* **29**, 877–894.
68 Fliesler SJ and Bretillon L (2010) The ins and outs of cholesterol in the vertebrate retina. *J Lipid Res* **51**, 3399–3413.
69 Ripps H and Shen W (2012) Review: taurine: a "very essential" amino acid. *Mol Vis* **18**, 2673–2686.
70 Lin CT, Song GX and Wu JY (1985) Ultrastructural demonstration of L-glutamate decarboxylase and cysteinesulfinic acid decarboxylase in rat retina by immunocytochemistry. *Brain Res* **331**, 71–80.
71 Lin CT, Li HZ and Wu JY (1983) Immunocytochemical localization of L-glutamate decarboxylase, gamma-aminobutyric acid transaminase, cysteine sulfinic acid decarboxylase, aspartate aminotransferase and somatostatin in rat retina. *Brain Res* **270**, 273–283.
72 Ganea E and Harding JJ (2006) Glutathione-related enzymes and the eye. *Curr Eye Res* **31**, 1–11.
73 Fujii T, Mori K, Takahashi Y, Taniguchi N, Tonosaki A, Yamashita H and Fujii J (2001) Immunohistochemical study of glutathione reductase in rat ocular tissues at different developmental stages. *Histochem J* **33**, 267–272.
74 Lu SC, Bao Y, Huang ZZ, Sarthy VP and Kannan R (1999) Regulation of gamma-glutamylcysteine synthetase subunit gene expression in retinal Muller cells by oxidative stress. *Invest Ophthalmol Vis Sci* **40**, 1776–1782.
75 Naash MI and Anderson RE (1989) Glutathione-dependent enzymes in intact rod outer segments. *Exp Eye Res* **48**, 309–318.

76 Naash MI, Nielsen JC and Anderson RE (1988) Regional distribution of glutathione peroxidase and Glutathione-S-transferase in adult and premature human retinas. *Invest Ophthalmol Vis Sci* **29**, 149–152.
77 Atalla L, Fernandez MA and Rao NA (1987) Immunohistochemical localization of catalase in ocular tissue. *Curr Eye Res* **6**, 1181–1187.
78 Armstrong D, Siakotos A, Koppang N and Connole E (1978) Studies on the retina and the pigment epithelium in hereditary canine ceroid lipofuscinosis, I. The distribution of enzymes in the whole retina and pigment epithelium. *Invest Ophthalmol Vis Sci* **17**, 608–617.
79 Ogawa T, Ohira A and Amemiya T (1997) Manganese and copper-zinc superoxide dismutases in the developing rat retina. *Acta Histochem* **99**, 1–12.
80 Kiser PD, Golczak M, Maeda A and Palczewski K (2012) Key enzymes of the retinoid (visual) cycle in vertebrate retina. *Biochim Biophys Acta* **1821**, 137–151.
81 Newsome DA, Fletcher RT and Chader GJ (1980) Cyclic nucleotides vary by area in the retina and pigmented epithelium of the human and monkey. *Invest Ophthalmol Vis Sci* **19**, 864–869.
82 Martinasevic MK, Green MD, Baron J and Tephly TR (1996) Folate and 10-formyltetrahydrofolate dehydrogenase in human and rat retina: relation to methanol toxicity. *Toxicol Appl Pharmacol* **141**, 373–381.
83 Davanger S, Ottersen OP and Storm-Mathisen J (1991) Glutamate, GABA, and glycine in the human retina: an immunocytochemical investigation. *J Comp Neurol* **311**, 483–494.
84 Bernard M, Donohue SJ and Klein DC (1995) Human hydroxyindole-O-methyltransferase in pineal gland, retina and Y79 retinoblastoma cells. *Brain Res* **696**, 37–48.
85 Rao GN and Cotlier E (1985) The enzymatic activities of GTP cyclohydrolase, sepiapterin reductase, dihydropteridine reductase and dihydrofolate reductase; and tetrahydrobiopterin content in mammalian ocular tissues and in human senile cataracts. *Comp Biochem Physiol B* **80**, 61–66.
86 Kaur J, Sawhney M, Dattagupta S, Shukla NK, Srivastava A and Ralhan R (2010) Clinical significance of phosphatidyl inositol synthase overexpression in oral cancer. *BMC Cancer* **10**, 168.
87 Willmon CL, Krabbenhoft E and Black ME (2006) A guanylate kinase/HSV-1 thymidine kinase fusion protein enhances prodrug-mediated cell killing. *Gene Ther* **13**, 1309–1312.
88 Niesporek S, Denkert C, Weichert W, Köbel M, Noske A, Sehouli J, Singer JW, Dietel M and Hauptmann S (2005) Expression of lysophosphatidic acid acyltransferase beta (LPAAT-beta) in ovarian carcinoma: correlation with tumour grading and prognosis. *Br J Cancer* **92**, 1729–1736.
89 Diefenbach CS, Soslow RA, Iasonos A, Linkov I, Hedvat C, Bonham L, Singer J, Barakat RR, Aghajanian C and Dupont J (2006) Lysophosphatidic acid acyltransferase-beta (LPAAT-beta) is highly expressed in advanced ovarian cancer and is associated with aggressive histology and poor survival. *Cancer* **107**, 1511–1519.
90 Pagel JM, Laugen C, Bonham L, Hackman RC, Hockenbery DM, Bhatt R, Hollenback D, Carew H, Singer JW and Press OW (2005) Induction of apoptosis using inhibitors of lysophosphatidic acid acyltransferase-beta and anti-CD20 monoclonal antibodies for treatment of human non-Hodgkin's lymphomas. *Clin Cancer Res* **11**, 4857–4866.
91 Springett GM, Bonham L, Hummer A, Linkov I, Misra D, Ma C, Pezzoni G, Di Giovine S, Singer J, Kawasaki H *et al.* (2005) Lysophosphatidic acid acyltransferase-beta is a prognostic marker and therapeutic target in gynecologic malignancies. *Cancer Res* **65**, 9415–9425.
92 Coon M, Ball A, Pound J, Ap S, Hollenback D, White T, Tulinsky J, Bonham L, Morrison DK, Finney R *et al.* (2003) Inhibition of lysophosphatidic acid acyltransferase beta disrupts proliferative and survival signals in normal cells and induces apoptosis of tumor cells. *Mol Cancer Ther* **2**, 1067–1078.
93 Hideshima T, Chauhan D, Hayashi T, Podar K, Akiyama M, Mitsiades C, MItsiades N, Gong B, Bonham L, de Vries P *et al.* (2003) Antitumor activity of lysophosphatidic acid acyltransferase-beta inhibitors, a novel class of agents, in multiple myeloma. *Cancer Res* **63**, 8428–8436.
94 Hu CM and Chang ZF (2008) Synthetic lethality by lentiviral short hairpin RNA silencing of thymidylate kinase and doxorubicin in colon cancer cells regardless of the p53 status. *Cancer Res* **68**, 2831–2840.
95 Brockmoller SF, Bucher E, Müller BM, Budczies J, Hilvo M, Griffin JL, Orešič M, Kallioniemi O, Iljin K, Loibl S *et al.* (2012) Integration of metabolomics and expression of glycerol-3-phosphate acyltransferase (GPAM) in breast cancer-link to patient survival, hormone receptor status, and metabolic profiling. *J Proteome Res* **11**, 850–860.
96 Marchan R, Büttner B, Lambert J, Edlund K, Glaeser I, Blaszkewicz M, Leonhardt G, Marienhoff L, Kaszta D, Anft M *et al.* (2017) Glycerol-3-phosphate acyltransferase 1 promotes tumor cell migration and poor survival in ovarian carcinoma. *Cancer Res* **77**, 4589–4601.
97 Hebrard C, Dumontet C and Jordheim LP (2009) Development of gene therapy in association with clinically used cytotoxic deoxynucleoside analogues. *Cancer Gene Ther* **16**, 541–550.
98 Lu Y, Wang W, Wang J, Yang C, Mao H, Fu X, Wu Y, Cai J, Han J, Xu Z *et al.* (2013) Overexpression of arginine transporter CAT-1 is associated with

accumulation of L-arginine and cell growth in human colorectal cancer tissue. *PLoS ONE* **8**, e73866.
99 Abdelmagid SA, Rickard JA, McDonald WJ, Thomas LN and Too CK (2011) CAT-1-mediated arginine uptake and regulation of nitric oxide synthases for the survival of human breast cancer cell lines. *J Cell Biochem* **112**, 1084–1092.
100 Bock AJ, Dong HP, Trope CG, Staff AC, Risberg B and Davidson B (2012) Nucleoside transporters are widely expressed in ovarian carcinoma effusions. *Cancer Chemother Pharmacol* **69**, 467–475.

Supporting information

Additional supporting information may be found online in the Supporting Information section at the end of the article.

Table S1. (A–B) Excel sheet containing gene expression profile of all the samples and their DESeq analysis.
Table S2. Reaction content of draft models, model curation, and final reaction contents.
Table S3. Excel sheet containing model details of the developed healthy and RB models.
Table S4. Excel sheet containing results of retina function tests of all the models
Table S5. Excel sheet containing secretion profiles of all the models.
Table S6. Excel sheet containing results of the synthetic lethal simulation
Table S7. Lipid composition of normal retina.
Doc S1. Summary of major metabolic pathways operating in healthy retina.